REPORT

TOPOLOGICAL MATTER

Observation of fractional Chern insulators in a van der Waals heterostructure

Eric M. Spanton,[1]* Alexander A. Zibrov,[2]* Haoxin Zhou,[2] Takashi Taniguchi,[3] Kenji Watanabe,[3] Michael P. Zaletel,[4] Andrea F. Young[2]†

Topologically ordered phases are characterized by long-range quantum entanglement and fractional statistics rather than by symmetry breaking. First observed in a fractionally filled continuum Landau level, topological order has since been proposed to arise more generally at fractional fillings of topologically nontrivial Chern bands. Here we report the observation of gapped states at fractional fillings of Harper-Hofstadter bands arising from the interplay of a magnetic field and a superlattice potential in a bilayer graphene–hexagonal boron nitride heterostructure. We observed phases at fractional filling of bands with Chern indices $\mathcal{C} = -1$, ±2, and ±3. Some of these phases, in $\mathcal{C} = -1$ and $\mathcal{C} = 2$ bands, are characterized by fractional Hall conductance—that is, they are known as fractional Chern insulators and constitute an example of topological order beyond Landau levels.

Bands in electronic systems can be classified by their symmetry and topology (1). In two dimensions with no symmetries beyond charge conservation, for example, bands are characterized by a topological Chern number, $\mathcal{C}$ (2). The Chern number determines the Hall conductance contributed by a filled band, which takes quantized integer values, $\sigma_{xy} = t\frac{e^2}{h}$ with $t \in \mathbb{Z}$ (2) (here e is the charge of an electron, h is the Planck constant, and $\mathbb{Z}$ is the set of all integers). Systems with an integer number of filled bands with nonzero $\mathcal{C}$ (Chern bands) thus show a quantized, nonzero Hall conductance and are known as Chern insulators (CIs). The first experimental examples of CIs are the integer quantum Hall (IQH) states, which have been observed in isotropic two-dimensional electron systems subjected to a large magnetic field (3). In the case of IQH states, a quantized Hall conductance is observed when an integer number of Landau levels (LLs) are filled, each with $\mathcal{C} = 1$.

IQH systems are very nearly translation-invariant, in which case t is fixed by the magnetic field B and the electron density n, via $t = \frac{nh}{Be}$, with some disorder required for the formation of plateaus in the Hall conductance (4). Recently, there has been interest in a different class of CIs for which continuous translation invariance is strongly broken by a lattice, decoupling the Hall conductance from the magnetic field. CIs in which t is decoupled from $\frac{n}{B}$ have been observed in magnetically doped thin films with strong spin-orbit interactions (5) and in the Harper-Hofstadter (2) bands of graphene subjected to a superlattice potential (6–8). Haldane's staggered flux model (9), which has nonzero quantized Hall conductance even when the net magnetic field is zero, has been engineered with ultracold atoms in an optical lattice (10).

Interactions expand the topological classification of gapped states, allowing t to be quantized to a rational fraction. By Laughlin's flux-threading argument, an insulator with $t = \frac{p}{q}$ (p, $q \in \mathbb{Z}$) must have a fractionalized excitation with charge $\frac{e}{q}$ (11). A fractionally quantized Hall conductance in a bulk insulator is thus a smoking-gun signature of topological order, and fractional quantum Hall (FQH) effects have been observed in partially-filled continuum LLs in a variety of experimental systems (12–15). Can a fractional Chern insulator (FCI) arise from fractionally filling a more general Chern band (16)? Although a FQH effect in a LL may be considered a special case of an FCI, in this work we focus on FCIs that require a lattice for their existence.

The phenomenology of lattice FCIs differs from that of continuum LLs. Chern bands with $\mathcal{C} \neq 1$ can arise, leading to different ground states than are allowed in $\mathcal{C} = 1$ LL. In addition, unlike LLs, Chern bands generically have a finite, tunable bandwidth that competes with interactions, providing a new setting for the study of quantum phase transitions. Finally, FCIs might be found in experimental systems where Chern bands, but not LLs, are realizable. A large body of theoretical work has begun to investigate these issues (17–24).

Here we report the experimental discovery of FCIs in a bilayer graphene (BLG) heterostructure at high magnetic fields. The requirements to realize an FCI in an experimental system are, first, the existence of a Chern band, and, second, electron-electron interactions strong enough to overcome both disorder and band dispersion. We satisfied these requirements by using a high-quality BLG heterostructure in which the bilayer is encapsulated between hexagonal boron nitride (hBN) gate dielectrics and graphite top and bottom gates (Fig. 1, A and B). This geometry was recently demonstrated to markedly decrease disorder, permitting the observation of delicate FQH states (25). We generated Chern bands by close rotational alignment (~1°) between the BLG and one of the two encapsulating hBN crystals. Beating between the mismatched crystal lattices leads to a long-wavelength (~10 nm) moiré pattern that the electrons in the closest layer experience as a periodic superlattice potential (Fig. 1B) (26). At high magnetic fields, the single-particle spectrum of an electron in a periodic potential forms the Chern bands of the Hofstadter butterfly (7–9). These bands are formally equivalent to Chern bands proposed to occur in zero magnetic field; at any fractional flux, a finite-field lattice model can be converted to an equivalent zero-field model using gauge invariance (16).

We measured the penetration field capacitance (27) (C_P), which distinguishes between gapped (incompressible) and ungapped (compressible) states (26). Figure 1, C and D, shows C_P measured as a function of B and the electron density, $n \approx n_0 \equiv c(v_t + v_b)$, where v_t and v_b are the applied top and bottom gate voltages and c denotes the geometric capacitance to either of the two symmetric gates. We used a perpendicular electric field, parameterized by $p_0/c = v_t - v_b$ (where p_0 is the electron density imbalance between layers in the absence of screening), to localize the charge carriers onto the layer with a superlattice potential, e.g., adjacent to the aligned hBN flake. High-C_P features, corresponding to gapped electronic states, are evident throughout the experimentally accessed parameter space (Fig. 1, C and D), following linear trajectories in the nB plane. We estimated the area of the superlattice unit cell from zero-field capacitance data (26) and defined the electron density $n_e = N_e/N_S$ and flux density $n_\Phi = N_\Phi/N_S$ per unit cell. Here N_e, N_S, and N_Φ are the number of electrons, superlattice cells, and magnetic flux quanta ($\Phi_0 = h/e$) in the sample, respectively. The trajectories are parameterized by their inverse slope t and n-intercept s in the nB plane.

$$N_e = tN_\Phi + sN_S, \quad n_e = tn_\Phi + s \qquad (1)$$

The Streda (28) formula, $t = \frac{\partial n_e}{\partial n_\Phi}\big|_{N_S} = \frac{h}{e^2}\sigma_{xy}$, shows that the Hall conductance of a gapped phase is exactly t. The invariant $s = \frac{\partial N_e}{\partial N_S}\big|_{N_{\Phi_0}}$ encodes the amount of charge "glued" to the unit cell; i.e., the charge that is transported if the lattice is dragged adiabatically (29). Nonzero s indicates that strong
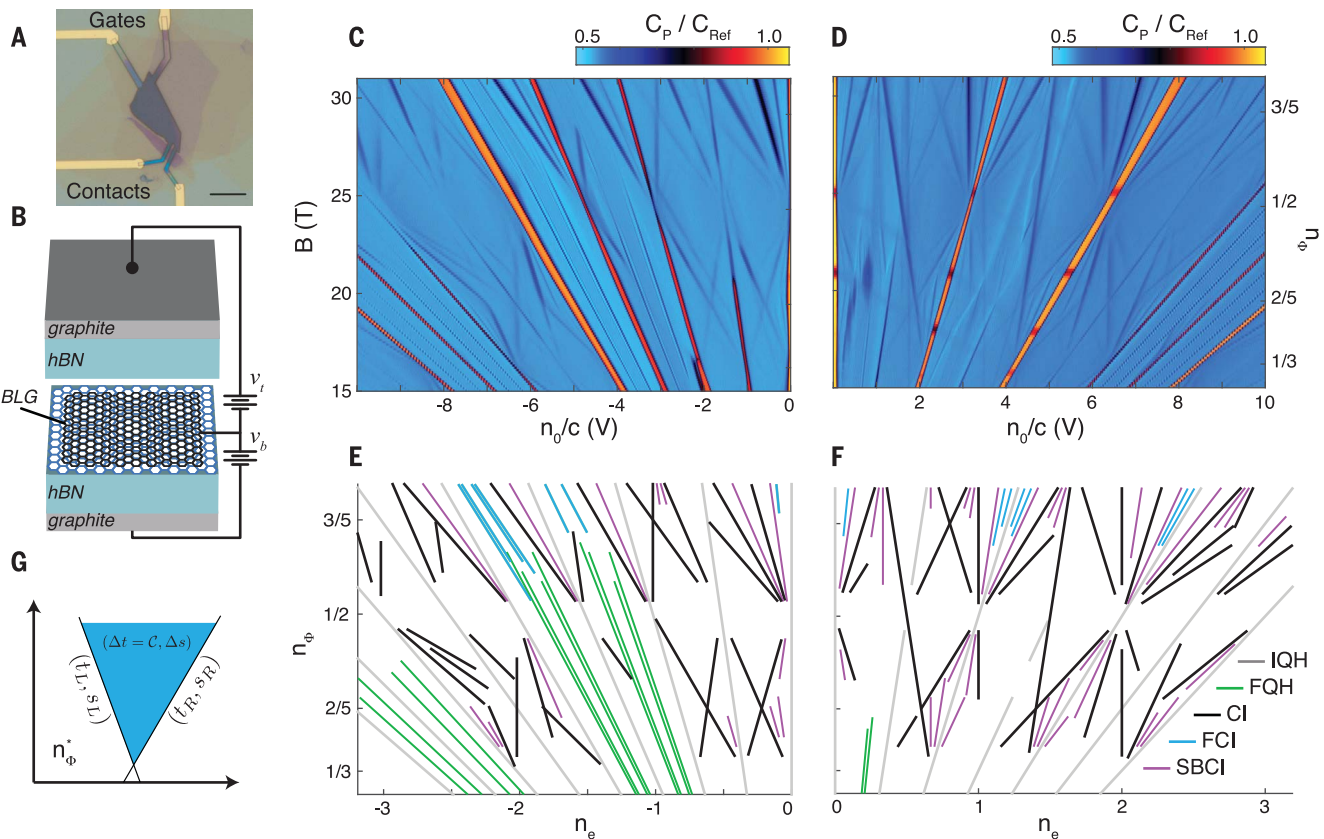
Fig. 1. Magnetocapacitance in a high-quality BLG moiré superlattice device. (**A**) Optical micrograph of the device. Scale bar, 10 μm. (**B**) Schematic of the device, with top and bottom graphite gates at potential v_t and v_b. A moiré potential is induced by alignment of the graphene bilayer with one of the encapsulating hBN crystals. (**C**) Penetration field capacitance (C_P) as a function of density $n_e \sim n_O \equiv c(v_t + v_b)$ and magnetic field B for $n_O < 0$. T = 300 mK, and C_{Ref} is a reference capacitance. A large electric field $p_O/c = (v_t - v_b) = 16$ V is applied to force the valence electrons onto the top layer, which is in contact with the aligned hBN. (**D**) C_P for $n_O > 0$ with $v_t - v_b = -16$ V at T = 300 mK. (**E** and **F**) Linear gap trajectories observed in (C) and (D)

parameterized by $n_e = t \cdot n_\Phi + s$. n_Φ and n_e are the magnetic flux quanta and number of electrons per moiré unit cell, respectively. $n_\Phi \equiv \frac{\sqrt{3}\lambda^2 B}{2\Phi_0} = 1/2$ (λ, wavelength) when B = 24.3 T and n_e = 1 when n_O/c = 3.1 V. Five trajectory classes are distinguished by color: Integer quantum Hall (gray; $s = 0$, $t \in \mathbb{Z}$), fractional quantum Hall (green; $s = 0$, t fractional), Hofstadter Chern insulators (black; $s, t \in \mathbb{Z}$, $s \neq 0$), symmetry-broken Chern insulators (purple; fractional s, $t \in \mathbb{Z}$), and fractional Chern insulators (cyan; fractional s, t). (**G**) Schematic of a ($\Delta t, \Delta s$) Chern band (see text).

lattice effects have decoupled the Hall conductance from the electron density. Within band theory, the invariants of a gap arise from summing the invariants (Δt_j, Δs_j) of the occupied bands, $(t, s) = \sum_{j \in occ} (\Delta t_j, \Delta s_j)$—in particular, the Hall conductance t is the sum of the occupied band Chern indices, $\Delta t_j = \mathcal{C}_j$.

On the basis of the properties of t and s, we observed five classes of high-C_P trajectories, each of which corresponds to a distinct class of gapped state (Fig. 1, E and F). Free-fermion band gaps must have integer t and s: Trajectories with $s = 0$ correspond to gaps between LLs, i.e., IQH states. Trajectories with $s \neq 0$ indicate the formation of the non-LL Chern bands of the Hofstadter butterfly (6–8). Trajectories with fractional t or s are beyond the single-particle picture and thus indicate interaction-driven gapped phases. The conventional FQH states follow trajectories with fractional t and $s = 0$. Gap trajectories with integer t and fractional s [previously

observed in monolayer graphene (30)] must be either topologically ordered or have interaction-driven spontaneous symmetry breaking of the superlattice symmetry. The theoretical analysis below suggests that the latter case is most likely, so we refer to this class as symmetry-broken Chern insulators (SBCIs). Finally, there are trajectories with fractional t and fractional s, which are the previously unreported class of topologically ordered FCI phases.

To better understand states with fractional t or s, we first identified the single-particle Chern bands in our experimental data by identifying all integer-t, integer-s gapped states. We focused on adjacent pairs of gapped states with integer (t_L, s_L) and (t_R, s_R) (where L and R denote gapped states with lower and higher n_O, respectively), which form the boundaries of a finite range of n_e in which no other single-particle gapped states appear (Fig. 1G). Adding charge to the left gapped state corresponds to filling a Chern band with invariants $(\Delta t, \Delta s) = (t_R - t_L, s_R - s_L)$. From

this criterion, we detected a variety of Chern bands with $\Delta t = \pm 1, \pm 2, \pm 3$, and ± 5 in the experimental data (26), each of which appears as a triangle between adjacent single-particle gapped states. These Chern bands are observed to obey certain rules expected from the Hofstadter problem: For example, Δt and Δs are always coprime, and Chern bands with Δt always emanate from a flux $n_\Phi^* = p/\Delta t$.

Interaction-driven phases occur at fractional filling v_C of a Chern band, following trajectories $(t_{v_C}, s_{v_C}) = (t_L, s_L) + v_C(\Delta t, \Delta s)$. The Chern numbers of the bands in which some of the observed interaction-driven phases appear (Fig. 2, A to C) are depicted schematically in Fig. 2, D to F.

By combining a phenomenological description of the moiré potential with knowledge of orbital symmetry breaking in BLG (31), we were able to construct a single-particle model that closely matches the majority of the experimentally observed single-particle Chern bands (25). The
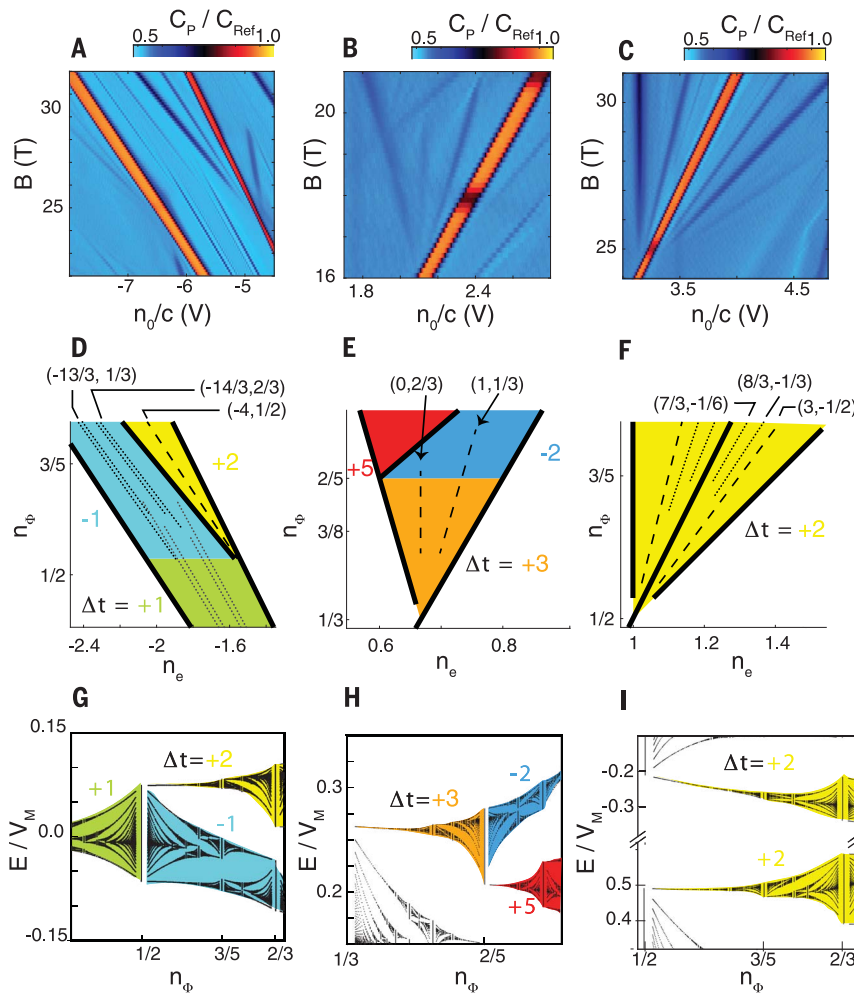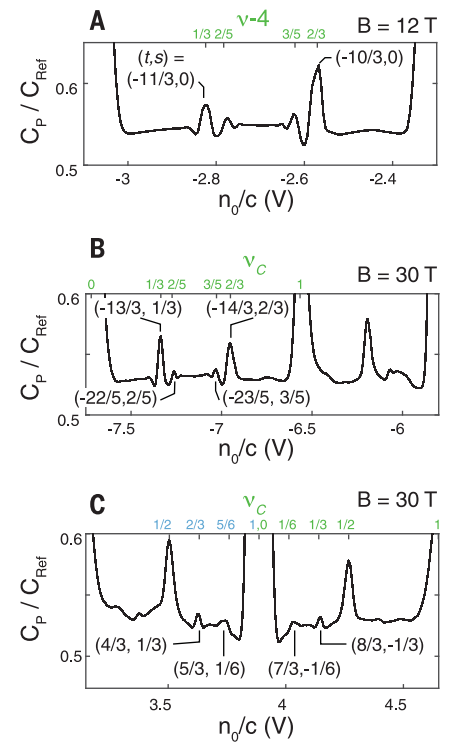
Fig. 2. Interaction-driven states at partial Chern-band filling. (**A** to **C**) Details of Fig. 1, C and D, showing (A) FCI states in a $\Delta t = -1$ band, (B) SBCI states in a $\Delta t = +3$ band, and (C) FCI and SBCI states in $\Delta t = 2$ bands. (**D**) Schematic of (A). FCI states (black dotted lines) with $(t, s) = (-13/3, 1/3)$, $(-22/5, 2/5)$, $(-23/5, 3/5)$, and $(-14/3, 2/3)$ occur at fractional filling of a $\Delta t = -1$ band (light blue). FQH states (gray dotted lines) occur at fractional filling of a conventional LL ($\Delta t = +1$, green) at low fields. (**E**) Schematic of (B). SBCI states (dashed lines) at $(t, s) = (0, 2/3)$ and $(1, 1/3)$ occur at 1/3 and 2/3 fractional filling of a $\Delta t = 3$ band (orange). (**F**) Schematic of (C). Both FCI and SBCI states (dotted and dashed lines, respectively) occur in the $\Delta t = 2$ bands. (**G**) Calculated Hofstadter energy spectrum (25) in the regime of (A), matching the observation that the LL splits into $\mathcal{C} = -1, 2$ bands. (**H**) Calculated Hofstadter spectrum in the regime of (B), matching the observed splitting of a $\mathcal{C} = 3$ band into $\mathcal{C} = 5, -2$ bands. (**I**) Calculated Hofstadter spectrum in the regime of (C). The IQH gap at $v = 2$ separates the two single-particle bands and is much larger than v_M.

Fig. 3. Line cuts of C_P comparing FCI and FQH states. (**A**) Line cut of C_P versus n_0/c (bottom axis) and Chern band filling factor (v_C, top axis). The data are averaged over $p_0/c \sim 1.0$ to 4.0 V at $B = 12$ T, showing FQH states in a conventional LL. At low fields, the effective moiré potential is weak, and FQH states are observed at filling factors $v - 4 = 1/3, 2/3$ as well as $2/5, 3/5$ of the $\Delta t = +1$ LL. (**B**) Line cut averaged over $p_0/c \sim 4.0$ to 14.0 V at $B = 30$ T, showing FCI in the $\Delta t = -1$ band (also shown in Fig. 2A). Weaker features appear at $v_C = 2/5, 3/5$, similar to the composite fermion sequence in (A). (**C**) Line cut averaged over $p_0/c \sim -14.0$ to 9.0 V at $B = 30$ T, showing FCI in two $\Delta t = 2$ bands (also shown in Fig. 2C). Blue and green values indicate the filling of two distinct bands. The relative strength of the $v_C = 1/3$ state compared to the $v_C = 1/6$ state in the right $\Delta t = 2$ band is consistent with the former preserving the lattice symmetry.

calculated energy spectra of the bands relevant to Fig. 2, A to C, are shown in Fig. 2, G to I. As is clear from the band structure, stable phases at fractional v_C are not expected within the single-particle picture: Instead, the encompassing Chern band splits indefinitely into finer Chern bands at lower levels of the fractal butterfly that depend sensitively on n_Φ.

The three columns of Fig. 2 represent instances of three general classes of fractional v_C states observed in our experiment. Figure 2A shows two gapped states within a $\Delta t = -1$ band at $v_C = \frac{1}{3}$ and $\frac{2}{3}$. These gapped states extend from $n\Phi \approx 0.55$ to at least $n_\Phi \approx 0.8$ (26). Both are characterized by fractional t and s, and we identify them as FCI

states. As with FQH states, the fractionally quantized Hall conductance implies that the system has a charge $e/3$ excitation (11). The fractional s values of these states, being multiples of this fractional charge, do not require broken superlattice symmetry. Gapped states at $v_C = 1/3, 2/3$ in a $\Delta t = -1$ band are accompanied by comparatively weaker states at $v_C = 2/5, 3/5$ (Fig. 3B). These fillings match the odd-denominator composite fermion sequence observed for FQH states (Fig. 3C), in agreement with theoretical predictions (32).

Figure 2 shows gapped states with fractional s and integer t at $v_C = 1/3, 2/3$ in a $\Delta t = +3$ band (Fig. 2B) and at $v_C = 1/2$ in a $\Delta t = +2$ band (Fig.

2C). Filling a Chern-Δt band to a multiple of $v_C = \frac{1}{|\Delta t|}$ corresponds to integer t but fractional s. These states are unlikely to admit a simple interpretation as FCIs; however, we cannot exclude exotic fractionalized states. Absent fractional excitations, a gapped state with fractional $s = \frac{x}{y}$ implies broken superlattice symmetry: The unit cell of such a phase must contain an integral number of electrons, and the smallest such cell contains y superlattice sites. Theoretically, such symmetry breaking is expected to arise spontaneously as a result of electronic interactions, in a lattice analog of quantum Hall ferromagnetism (33). A Δt Chern band is similar to a Δt-component LL, but in contrast to an internal spin, translation acts by

cyclically permuting the components (33–35). Spontaneous polarization into one of these components thus leads to a t-fold increase of the unit cell (33). The observation of SBCIs is thus analogous to the observation of strong odd-integer IQHEs that break spin-rotational invariance. Some of the "fractional fractal" features recently described in monolayer graphene appear to be consistent with this explanation (30).

Further, we also observed fractional-t states within a $\Delta t = +2$ band (Fig. 3C); for example, at $v_C = 1/3$ ($t = 8/3$ and $s = -1/3$) and $v_C = 1/6$ ($t = 7/3$ and $s = -1/6$). FCIs in Chern–$\Delta t \neq \pm 1$ bands can either preserve or break the underlying lattice symmetry. Symmetry-preserving FCIs are expected (21, 32, 36) at fillings $v_C = \frac{m}{2lm\Delta t + 1}$ for integers l and m. The state observed at $v_C = 1/3$ is consistent with this sequence ($l = 1$, $m = -1$); in contrast, the weaker state at $v_C = 1/6$ is not. For the $v_C = 1/6$ state, the observed $t = 7/3$ suggests a fundamental charge of $e/3$. As for SBCIs, the observed $s = -1/6$ implies that each unit cell binds only half a fundamental charge—i.e., the moiré unit cell is doubled and the $v_C = 1/6$ state is a symmetry-broken FCI state. A $\Delta t = 2$ Hofstadter band is similar to a spin-degenerate LL, with lattice symmetry taking the place of spin symmetry. In a spin-degenerate LL at $v_C = 1/6$ (i.e., LL filling $v_C = 1/3$), the system spontaneously spin polarizes, forming a single-component Laughlin state. In contrast, at $v_C = 1/3$ ($v_C = 2/3$) the system can either spin polarize (observed only for large Zeeman energy) or form a multicomponent FQH state that preserves spin rotation symmetry. The absence of an obvious analog of the Zeeman effect in our Hofstadter band makes a multicomponent state a more likely candidate for the feature observed at $v_C = 2/3$.

To assess the plausibility of FCI and SBCI ground states, we used the infinite density matrix renormalization group (iDMRG) to numerically compute the many-body ground state within a minimal model of the BLG (37). We first considered Coulomb interactions and a triangular moiré potential of amplitude V_M projected into a BLG $N = 0$ LL (38), matching the parameter regime in Fig. 2A (26). We focused on $n_\Phi = \frac{2}{3}$ at a density corresponding to $v_C = \frac{1}{3}$ filling of the $\Delta t = -1$ band.

If interactions are too weak compared with the periodic potential [as parameterized by V_M/E_C, where $E_C = e^2/(\varepsilon \ell_B)$ is the Coulomb energy, $\ell_B = \sqrt{\frac{h}{eB}}$ is the magnetic length, ε is the dielectric constant, and h is the reduced Planck constant], the ground state at $n_\Phi = \frac{2}{3}$ is gapless, corresponding to a partially filled Chern band. If the interactions are too strong, the system forms a Wigner crystal that is pinned by the moiré potential. In the intermediate regime, however, the numerical ground state of this model has a fractional t and s that match the experiment and hence is an FCI, with entanglement signatures that indicate a Laughlin-type topological order (26). The FCI is stable across a range of V_M/E_C (Fig. 4A) corresponding to $|V_M| \approx 14 - 38$ meV,

consistent with recent experiments (39) suggesting that $|V_M| \sim 25$ meV. Figure 4B shows that the real-space density of an FCI is strongly modulated by the potential but preserves all the symmetries of the superlattice.
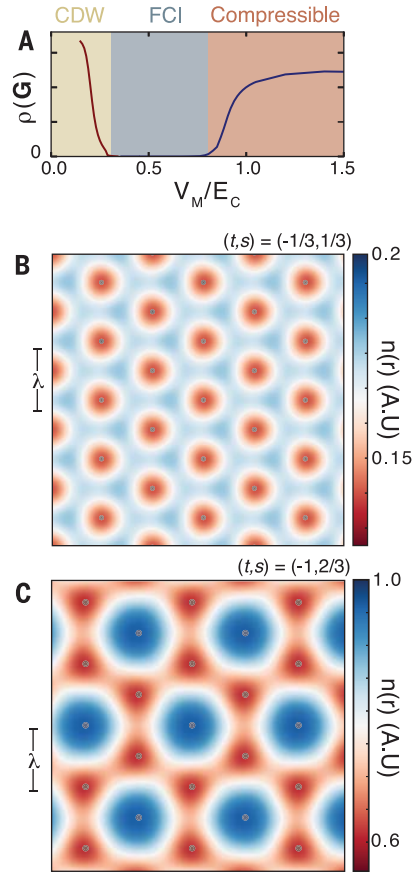
Fig. 4. iDMRG calculations showing the stability of FCI and SBCI states.
(**A**) Calculated iDMRG phase diagram at $v_C = 1/3$ filling of the $\Delta t = -1$ band shown in Fig. 2, A, D, and G ($n_\Phi = 2/3$). V_M is the moiré potential amplitude, E_C is the Coulomb energy, and $\rho(\mathbf{G})$ is the charge density at Bragg vector $\mathbf{G}$. The FCI competes with two other phases: a charge density wave (CDW) at low V_M and a compressible phase at high V_M. The competing phases are diagnosed by symmetry-breaking density waves at wave vector $\mathbf{G} = \mathbf{G}_0/3$ (red) and $\mathbf{G} = \mathbf{G}_0/2$ (blue), where $\mathbf{G}_0$ is a reciprocal vector of the moiré potential (25). (**B**) Calculated real-space electron density $n(r)$ of the FCI found in (A). $n(r)$ preserves the symmetry of the moiré potential, whose periodicity is indicated by the gray circles. Here $V_M/E_C = 0.7$. (**C**) Calculated real-space electron density $n(r)$ at $v_C = \frac{2}{3}$ filling of the $\Delta t = 3$ band shown in Fig. 2, B, E, and H ($n_\Phi = 3/8$). The result is consistent with an SBCI phase; $(t, s) = (-1, 2/3)$, and $n(r)$ spontaneously triples the unit cell of the underlying moiré potential, indicated by gray circles. Here $V_M/E_C = 0.6$ and $\Theta_M = \pi/8$.

We next conduct iDMRG calculations to assess the plausibility of the SBCI hypothesis. We focus on the well-developed Chern-3 band of Fig. 2, B, E, and H. As a minimal model, we project the moiré and Coulomb interactions into the $N = 1$ LL of the BLG, fixing $V_M = 21$ meV and $E_C(B = 17T) = 35$ meV, and take $n_\Phi = \frac{3}{8}$.

At $v_C = \frac{1}{3}$ filling, the electron density exhibits a modulation that spontaneously triples the superlattice unit cell (Fig. 4C). A similar tripling is observed at $v_C = \frac{2}{3}$. These are not merely density waves, however, as they have finite (t, s) invariants, in agreement with experimental observations.

The SBCI states are distinct from a second class of integer-t, fractional-s features, the moiré-pinned Wigner crystals (30, 40). In the latter case, starting from a LL-gap at $t, s = t_L, 0$, additional electrons form a Wigner crystal pinned by the moiré potential; the added electrons are electrically inert, leading to a state at $t, s = t_L, \frac{x}{y}$ that cannot be ascribed to fixed v_C of an encompassing band. These states are thus analogous to reentrant IQH effects, with the moiré potential playing the role of disorder. In contrast, although the electrons added to the SBCI spontaneously increase the unit cell, they also contribute an integer Hall conductance, which together corresponds to some v_C.

In summary, we find that instead of a self-repeating fractal structure, interactions mix Hofstadter-band wave functions to form stable, interaction-driven states at fractional filling of a Chern band. Among these are both SBCIs and topologically ordered FCIs, the latter of which constitute a lattice analog of the FQH effect. Lattice engineering can lead to increased experimental control. For example, multicomponent FCI states in bands with higher Chern numbers—as may be responsible for the $v_C = 1/3$ feature in Fig. 3C—have been predicted to host non-abelian defects at engineered lattice dislocations (34). A pressing experimental question, then, is whether FCI states can be realized in microscopically engineered superlattices.

REFERENCES AND NOTES
1. S. Ryu, A. P. Schnyder, A. Furusaki, A. W. W. Ludwig, *New J. Phys.* **12**, 065010 (2010).
2. D. J. Thouless, M. Kohmoto, M. P. Nightingale, M. den Nijs, *Phys. Rev. Lett.* **49**, 405–408 (1982).
3. K. Klitzing, G. Dorda, M. Pepper, *Phys. Rev. Lett.* **45**, 494–497 (1980).
4. S. M. Girvin, *Topological Aspects of Low Dimensional Systems* (Springer, 1999).
5. C.-Z. Chang et al., *Science* **340**, 167–170 (2013).
6. C. R. Dean et al., *Nature* **497**, 598–602 (2013).
7. L. A. Ponomarenko et al., *Nature* **497**, 594–597 (2013).
8. B. Hunt et al., *Science* **340**, 1427–1430 (2013).
9. F. D. M. Haldane, *Phys. Rev. Lett.* **61**, 2015–2018 (1988).
10. G. Jotzu et al., *Nature* **515**, 237–240 (2014).
11. R. B. Laughlin, *Phys. Rev. Lett.* **50**, 1395–1398 (1983).
12. D. C. Tsui, H. L. Stormer, A. C. Gossard, *Phys. Rev. Lett.* **48**, 1559–1562 (1982).
13. X. Du, I. Skachko, F. Duerr, A. Luican, E. Y. Andrei, *Nature* **462**, 192–195 (2009).
14. K. I. Bolotin, F. Ghahari, M. D. Shulman, H. L. Stormer, P. Kim, *Nature* **462**, 196–199 (2009).
15. A. Tsukazaki et al., *Nat. Mater.* **9**, 889–893 (2010).
16. We use the term "fractional Chern insulator" to denote any non-FQH, topologically ordered state

at fractional filling of a Chern band, rather than a more restrictive definition requiring the states to occur at zero field.

17. S. A. Parameswaran, R. Roy, S. L. Sondhi, *C. R. Phys.* **14**, 816–839 (2013).
18. E. J. Bergholtz, Z. Liu, *Int. J. Mod. Phys. B* **27**, 1330017 (2013).
19. A. S. Sørensen, E. Demler, M. D. Lukin, *Phys. Rev. Lett.* **94**, 086803 (2005).
20. R. N. Palmer, D. Jaksch, *Phys. Rev. Lett.* **96**, 180407 (2006).
21. G. Möller, N. R. Cooper, *Phys. Rev. Lett.* **115**, 126401 (2015).
22. D. N. Sheng, Z.-C. Gu, K. Sun, L. Sheng, *Nat. Commun.* **2**, 389 (2011).
23. T. Neupert, L. Santos, C. Chamon, C. Mudry, *Phys. Rev. Lett.* **106**, 236804 (2011).
24. N. Regnault, B. A. Bernevig, *Phys. Rev. X* **1**, 021014 (2011).
25. A. A. Zibrov *et al.*, *Nature* **549**, 360–364 (2017).
26. See supplementary materials.
27. J. P. Eisenstein, L. N. Pfeiffer, K. W. West, *Phys. Rev. Lett.* **68**, 674–677 (1992).
28. P. Streda, *J. Phys. C* **15**, L717–L721 (1982).
29. A. H. MacDonald, *Phys. Rev. B* **28**, 6713–6717 (1983).
30. L. Wang *et al.*, *Science* **350**, 1231–1234 (2015).
31. B. M. Hunt *et al.*, *Nat. Commun.* **8**, 948 (2017).
32. A. Kol, N. Read, *Phys. Rev. B* **48**, 8890–8898 (1993).
33. A. Kumar, R. Roy, S. L. Sondhi, *Phys. Rev. B* **90**, 245106 (2014).
34. M. Barkeshli, X.-L. Qi, *Phys. Rev. X* **2**, 031013 (2012).
35. Y.-L. Wu, N. Regnault, B. A. Bernevig, *Phys. Rev. Lett.* **110**, 106802 (2013).
36. A. Sterdyniak, C. Repellin, B. A. Bernevig, N. Regnault, *Phys. Rev. B* **87**, 205137 (2013).
37. M. P. Zaletel, R. S. K. Mong, F. Pollmann, E. H. Rezayi, *Phys. Rev. B* **91**, 045115 (2015).
38. X. Chen, J. R. Wallbank, M. Mucha-Kruczyński, E. McCann, V. I. Fal'ko, *Phys. Rev. B* **94**, 045442 (2016).
39. M. Lee *et al.*, *Science* **353**, 1526–1529 (2016).
40. A. M. DaSilva, J. Jung, A. H. MacDonald, *Phys. Rev. Lett.* **117**, 036802 (2016).

ACKNOWLEDGMENTS

SUPPLEMENTARY MATERIALS

Science

Observation of fractional Chern insulators in a van der Waals heterostructure

Eric M. Spanton, Alexander A. Zibrov, Haoxin Zhou, Takashi Taniguchi, Kenji Watanabe, Michael P. Zaletel and Andrea F. Young

Beyond fractional quantum Hall

Unlike most electronic topological phenomena, the fractional quantum Hall effect requires correlations among electrons. Spanton *et al.* describe a class of related but even more unusual states, the fractional Chern insulators (see the Perspective by Repellin and Regnault). They observed these states in samples of bilayer graphene, where one of the graphene layers was misaligned by a small angle with respect to an adjoining layer of hexagonal boron nitride. The misalignment created a superlattice potential and topologically nontrivial bands, which had a fractional filling, thanks to strong electronic interactions. The findings expand the class of correlated topological states, which have been predicted to harbor exotic excitations.

Science, this issue p. 62; see also p. 31

ARTICLE TOOLS	http://science.sciencemag.org/content/360/6384/62
SUPPLEMENTARY MATERIALS	http://science.sciencemag.org/content/suppl/2018/02/28/science.aan8458.DC1
RELATED CONTENT	http://science.sciencemag.org/content/sci/360/6384/31.full
REFERENCES	This article cites 58 articles, 5 of which you can access for free http://science.sciencemag.org/content/360/6384/62#BIBL
PERMISSIONS	http://www.sciencemag.org/help/reprints-and-permissions